

A Method to Estimate the Probability That Any Individual Cloud-to-Ground Lightning Stroke Was Within Any Radius of Any Point

Lisa L. Huddleston
NASA, Kennedy Space Center, Florida

William P. Roeder
45th Weather Squadron, Patrick AFB, Florida

Francis J. Merceret
NASA, Kennedy Space Center, Florida

Abstract

A new technique has been developed to estimate the probability that a nearby cloud-to-ground lightning stroke was within a specified radius of any point of interest. This process uses the bivariate Gaussian distribution of probability density provided by the current lightning location error ellipse for the most likely location of a lightning stroke and integrates it to determine the probability that the stroke is inside any specified radius of any location, even if that location is not centered on or even within the location error ellipse. This technique is adapted from a method of calculating the probability of debris collision with spacecraft (Alfano 2007, Alfano 2009, Chan 2008). Such a technique is important in spaceport processing activities because it allows engineers to quantify the risk of induced current damage to critical electronics due to nearby lightning strokes. This technique was tested extensively and is now in use by space launch organizations at Kennedy Space Center and Cape Canaveral Air Force station.

1. Introduction

The estimation of the probability of an individual nearby cloud-to-ground lightning stroke was within a specified distance of any specified spaceport processing facility at Kennedy Space Center (KSC) or Cape Canaveral Air Force Station (CCAFS) is important. This estimate allows engineers to decide if inspection of electronics of satellite payloads, space launch vehicles, and ground support equipment for damage from induced currents from that stroke is warranted. If induced current damage has occurred, inspections of the electronics are critical to identify required fixes and avoid degraded performance or failure of the satellite or space launch vehicle. However, inspections are costly both financially and in terms of delayed processing for space launch activities. As such, it is important these inspections be avoided if not needed. At KSC/CCAFS, one of the main purposes of the Four Dimensional Lightning Surveillance System (4DLSS) (Murphy et al. 2008, Roeder 2010) is detection of nearby strokes and determination of their peak current to support those inspection decisions (Flinn et al 2010a, Flinn et al 2010b, Roeder et al 2005). The high frequency of occurrence of lightning in East Central Florida combined with the large amount of complex sensitive electronics in satellite payloads, space launch vehicles, and associated facilities make those decisions critically important to space launch processing. While 4DLSS provides the data for 50th percentile location error ellipses for the best location for each stroke, which is then scaled to 95th or 99th percentile ellipses depending on customer, it has not been able to provide the probability for the stroke being within a customer specified distance of a point of interest. This paper presents a new method to convert the 4DLSS 50th percentile location error

ellipse for best location of any stroke into the probability that the stroke was within any radius of any facility at CCAFS/KSC. This new facility-centric technique is a significant improvement over the stroke-centric location error ellipses the 45th Weather Squadron (45WS) has provided in the past. This technique is adapted from a method of calculating the probability of debris collision with spacecraft (Alfano 2007, Alfano 2009, Chan 2008, Leleux 2002).

2. Background

In spacecraft collision probability and the other applications, at the instant of “nominal” closest approach, the position uncertainty of the collision object relative to the asset is described by a bivariate Gaussian probability density function (pdf) (Alfano 2007, Alfano 2009, Chan 2008), as shown in the following equation.

$$f_2(x, z) = \frac{1}{2\pi\sigma_x\sigma_z\sqrt{1-\rho_{xz}^2}} e^{-\left[\left(\frac{x}{\sigma_x}\right)^2 - 2\rho_{xz}\left(\frac{x}{\sigma_x}\right)\left(\frac{z}{\sigma_z}\right) + \left(\frac{z}{\sigma_z}\right)^2\right]/2(1-\rho_{xz}^2)} \quad (1)$$

where σ_x and σ_z = the standard deviations of x and z, ρ_{xz} = correlation coefficient of x and z, x and z are the designations for the rectangular coordinates in the collision plane. The probability of collision is given by the two-dimensional integral, where A is the collision cross-sectional area which is a circle with radius, r_A (Chan 2008).

$$P = \iint_A f_2(x, z) dx dz \quad (2)$$

There is no known analytical solution to the above integral when the two standard deviations σ_x and σ_z are not equal. The solution is based either on transforming the two dimensional Gaussian probability distribution function (pdf) to a one-dimensional Rician pdf and using the concept of equivalent areas or by performing a numerical integration of the two dimensional Gaussian pdf (Alfano 2007, Alfano 2009, Chan 2008).

The geometry used for spaceflight collision probability can also be used for estimation of the probability of an individual nearby lightning stroke contacting the surface within a specified distance of a specified point of interest as shown in Figure 1. Both solution methods, numerical integration as well as the analytical method of equivalent areas using the Rician pdf, will be analyzed in the next section.

3. Evaluation

The probability that any lightning strike is within any radius of any point of interest would be extremely difficult to estimate intuitively. As a result, given the high impact of the decisions on space launch operations, the tool must be extensively tested. Three major types of tests were conducted and are discussed in the following sections: 1) known mathematical solutions, 2) expected behavior as single parameters are varied, and 3) examination of real-world events. The new technique passed all of the tests.

a. Test Set 1

The first set of testing compared the probability calculated by the program to the corresponding circular probability from the CRC Handbook of Tables for Probability and Statistics. (Beyer *ed.* 1968) Table 1 shows the probability from the new technique for

various inputs and the corresponding correct probability from the CRC Handbook. The values matched to within a tenth of a percent. These differences in the final digit may be due to round-off error.

b. Test Set 2

The second type of testing involved plotting the calculated probabilities as particular inputs were varied while holding the other inputs constant and comparing them to an independently coded program written by Dr. F. Kenneth Chan of the Aerospace Corporation and the author of "Spacecraft Collision Probability" (Chan 2008). Also tested was the difference between using a numerical integration technique for calculating the probability versus an analytical technique, shown as "Rician" in the results below. The analytical or Rician technique involves transforming the two dimensional Gaussian pdf to a one-dimensional Rician pdf and using the concept of equivalent areas to calculate the probability (Alfano 2007, Alfano 2009, Chan 2008). The results are shown in Figures 2 through 5 and 8. The data used to generate these figures are in Table 2. Note that results using the 45WS and Chan's program match almost exactly regardless of integration method used. Probability calculations are much faster using the analytical technique as opposed to the numerical integration technique. Since 45WS must sometimes process thousands of lightning strokes after intense local lightning events, it was of interest to understand the conditions in which the analytical technique performed well compared to the numerical integration technique. The numerical integration technique and the analytical integration technique tend to diverge as the ratio of the semi-major axis to

semi-minor axis increases and as the orientation angle of the ellipse approaches 0 or 180 degrees.

Figure 2 shows the change in probability as a result of changing the radius around the point of interest while holding all other parameters constant. Chan's probability calculated using both the numerical integration technique as well as the analytical (Rician) technique is compared to the probability calculated using the 45WS program. The worst case probability difference between methods is 0.25% at a radius of 2 nautical miles around the point of interest. Chan's probability using both techniques matches the 45WS probability exactly at all radii.

Figure 3 shows the change in probability as a result of changing the latitude of the strike from the point of interest while holding all other parameters constant. Chan's probability calculated using both the numerical integration technique as well as the analytical (Rician) technique is compared to the probability calculated using the 45WS program. The probability follows a Gaussian curve and reaches a maximum when the uncertainty ellipse is at its closest point of approach to the point of interest, as expected. The worst case probability difference between methods is 0.06 where the lightning stroke is at latitude of 28.6162°N, which is about 0.5 nautical miles away from the point of interest. Chan's probability using both techniques matches the 45WS probability exactly at all latitudes.

Figure 4 shows the change in probability as a result of changing the longitude of the strike from the point of interest while holding all other parameters constant. Chan's probability calculated using both the numerical integration technique as well as the analytical (Rician) technique is compared to the probability calculated using the 45WS

program. The probabilities follow a Gaussian curve and reach a maximum when the uncertainty ellipse is at its closest point of approach to the point of interest, as expected. The worst case probability difference between methods is 0.08 where the lightning stroke is at a longitude of 80.5961°W , which is about 0.4 nautical miles away from the point of interest. Chan's probability using both techniques matches the 45WS probability exactly at all longitudes.

Figure 5 shows the change in probability as a result of changing the heading from true north of the semi-major axis of the lightning uncertainty ellipse while holding all other parameters constant. Chan's probability calculated using both the numerical integration technique as well as the analytical (Rician) technique is compared to the probability calculated using the 45WS program. The center of the stroke uncertainty ellipse is located about 0.5 nautical miles away from the point of interest. The probabilities show a roughly sinusoidal pattern as more, then less, then more of the ellipse rotates into, out of, then into the area around the point of interest. However, the difference in probability between the two integration techniques is enhanced as the ellipse is rotated. The worst case probability difference between methods is 0.28 where the lightning stroke heading is at an angle of 0° or 180° from true north.

Figures 6 and 7 show a Google Maps visualization of the 99% confidence lightning uncertainty ellipse as it is rotated from 180° to 90° from true north. The lightning uncertainty ellipse at a heading of 90° from true north is the rotation angle at which there is no difference in the probability calculated by the numerical integration technique and the analytical (Rician) technique. Chan's probability using both techniques matches the 45WS probability exactly at all angles.

Figure 8 shows the change in probability as a result of varying the aspect ratio (length of semi-major axis/length of semi-minor axis) of the lightning uncertainty ellipse from 1.5 to 11 with the strike point close to the point of interest while holding all other parameters constant. Chan's probability calculated using both the numerical integration technique as well as the analytical (Rician) technique is compared to the probability calculated using the 45WS program. The probability becomes less as the aspect ratio of the uncertainty ellipse is larger. However, the difference in probability between the two integration techniques is enhanced as the aspect ratio is increased. The worst case probability difference between methods is 0.07 where the aspect ratio is 8. Chan's probability using both techniques matches the 45WS probability exactly at all aspect ratios.

In light of the results of the differences between calculations (numerical integration vs. analytical [Rician] method), the 45WS decided to use the numerical integration technique to calculate probabilities. Although the program run time is longer using the numerical integration technique, the accuracy improvements justify the longer calculation time.

c. Test Set 3

The third type of testing analyzed six real-world lightning strikes near Space Launch Complex 39A on 3 August 2009. Figure 9 shows the spreadsheet used to generate the lightning report for those six strikes. Additional data on these strikes are in Table 3. These strikes were selected because the closest point on the lightning position uncertainty ellipse was within 0.45 nautical miles of Launch Complex 39A, the key

radius for assessing the need to inspect electronics for induced current damage to the Space Shuttle. Figures 10 through 15 are Google Maps depictions of these six strokes. The probabilities for a small area around a facility, even for a nearby stroke, may appear to be surprisingly low. For example, one strike just 0.65 nautical miles away (Figure 14) had only a 0.7% probability of being within the 0.45 nautical mile radius of Launch Complex 39A. All calculated probabilities are consistent with these real-world events.

The KSC Electromagnetic Environmental Effects (EEE) Panel requested six more real-world lightning strikes be investigated. These were recently investigated lightning strikes near Launch Complexes 39A or 39B where there was camera verification of the location of the strike. The EEE Panel wanted to compare the results of the new facility-centric probabilistic technique to these cases where the true answers were known unambiguously. The data used for this analysis are in Table 4. Both Cloud to Ground Lightning Surveillance System (CGLSS) and National Lightning Data Network (NLDN) cases were examined, depending upon which sensor system recorded the stroke. CGLSS strokes were obtained from 45WS 4DLSS and NLDN reports were purchased as special StrikeNet reports from Vaisala Corporation. Figures 16 through 21 show the probability results from these cases. As with the previous real-world tests, all calculated probabilities were consistent with these additional real-world events.

4. Summary

A technique has been developed to calculate the probability that any nearby cloud-to-ground lightning stroke was within any radius of any point of interest. In

practice, this provides the probability that a nearby lightning stroke was within a key distance of a facility, rather than the error ellipses centered on the stroke. This process uses the bivariate Gaussian distribution of probability density provided by the current lightning location error ellipse for the most likely location of a lightning stroke and integrates it to determine the probability that the stroke is inside any specified radius. This new facility-centric technique was tested extensively and is much more useful to the space launch customers and is superseding the lightning error ellipse approach discussed in Flinn et al 2010a, Flinn et al 2010b.

Acknowledgments.

This work would not exist were it not for the generous contributions and suggestions by Dr. Ken Chan of the Aerospace Corp, who is an expert on spacecraft collision probability, on whose work the probability of lightning within a radius of interest was based. Dr. Darrin Leleux of the Johnson Space Center, Houston, TX, and Dr. Walt Gill of Sandia National Laboratory also provided helpful guidance and testing. Mr. Jeremy Hinkley and Mr. Pete Hopman of United Space Alliance, the prime contractor for Space Shuttle operations, provided very valuable efficiency modifications for the visual basic code and also integrated the probability calculations and closest ellipse point algorithm into the 45th Weather Squadron Lightning Report Spreadsheet. The authors appreciate a helpful review of an earlier draft of this paper by Mr. John Madura of the Kennedy Space Center. This work was done under the Kennedy Space Center Employee Development Program.

References

Alfano, S., 2007: "Review of Conjunction Probability Methods for Short-term Encounters" AAS Paper No. 07-148, *AAS/AIAA Space Flight Mechanics Meeting*, Sedona, Arizona, 28 January-01 February 2007.

Alfano, S., 2009: "Satellite Collision Probability Enhancements" *J. Guidance, Control, and Dynamics*, **29**(3), 588-592.

Chan, F. Kenneth, 2008. *Spacecraft Collision Probability*. The Aerospace Press, El Segundo, CA.

CRC Handbook of Tables for Probability and Statistics, 2nd edition, 1968: W. H. Beyer, editor, Cleveland, OH: The Chemical Rubber Co., 151-157.

Flinn, F. C., W. P. Roeder, M. D. Buchanan, and T. M. McNamara, 2010a: Lightning Reporting at 45th Weather Squadron: Recent Improvements, *21st International Lightning Detection Conference*, 19-20 Apr 10, 18 pp..

Flinn, F. C., W. P. Roeder, D. F. Pinter, S. M. Holmquist, M. D. Buchanan, T. M. McNamara, M. McAleenan, K. A. Winters, P. S. Gemmer, M. E. Fitzpatrick, and R. D. Gonzalez, 2010b: Recent Improvements in Lightning Reporting At 45th Weather Squadron, *14th Conference on Aviation, Range, and Aerospace Meteorology*, 17-21 Jan 10, Paper 7.3, 14 pp.

Leleux, D., et. al., 2002: Probability-based Space Shuttle collision avoidance, *Space Ops 2002 Conference*, 20-24 Oct 2002, 18 pp.

Murphy, M. J., K. L. Cummins, N. W. S. Demetriades, and W. P. Roeder, 2008: Performance Of The New Four-Dimensional Lightning Surveillance System (4DLSS) At The Kennedy Space Center/Cape Canaveral Air Force Station Complex, *13th Conference on Aviation, Range, and Aerospace Meteorology*, 20-24 Jan 07, 18 pp.

Roeder, W. P., 2010: The Four Dimension Lightning Surveillance System. *21st International Lightning Detection Conference*, 21-22 Apr 10, 15 pp..

Roeder, W. P., J. W. Weems, and P. B. Wahner, 2005: Applications of the Cloud-To-Ground-Lightning-Surveillance-System Database. *1st Conference on Meteorological Applications of Lightning Data*, 9-13 Jan 05, 5 pp.

List of Figures

FIG. 1. Schematic diagram of the angles used in probability calculation for a sample lightning location error ellipse. α is the heading of the semi-major axis of the lightning location uncertainty ellipse from true north. θ is the angle between the semi-major axis of the lightning location uncertainty ellipse and line connecting the center of the lightning uncertainty ellipse and the center of the area of interest.

FIG. 2. Change in probability as a result of changing the point of interest radius while holding all other parameters constant.

FIG. 3. Change in probability as a result of changing the latitude of the strike from the point of interest while holding all other parameters constant.

FIG. 4. Change in probability as a result of changing the longitude of the strike from the point of interest while holding all other parameters constant.

FIG. 5. Change in probability as a result of changing the semi-major axis heading of the lightning uncertainty ellipse while holding all other parameters constant.

FIG. 6. Google Maps visualization of a lightning uncertainty ellipse overlaid on the radius around the point of interest with a semi-major axis heading of 180° as graphed in Figure 5.

FIG. 7. Google Maps visualization of a lightning uncertainty ellipse overlaid on the radius around the point of interest with a semi-major axis heading of 90° as graphed in Figure 5.

FIG. 8. Change in probability as a result of varying the aspect ratio (length of semi-major axis/length of semi-minor axis) of the lightning uncertainty ellipse from 1.5 to 11 with the strike point close to the point of interest while holding all other parameters constant.

FIG. 9. Sample of lightning strikes where the closest point on the lightning position uncertainty ellipse was within 0.45 nmi of Launch Complex 39A on 3 August 2009.

FIG. 10. Google Maps visualization of the 99% confidence uncertainty ellipse for the closest lightning strikes to Complex 39A on 03 August 2009. There is a 45.9% probability that the lightning strike occurred within the 0.45 nmi radius.

FIG. 11. Google Maps visualization of the 99% confidence uncertainty ellipse for one of the closest lightning strikes to Complex 39A on 03 August 2009. The center of the ellipse was within the 0.45 nmi radius. There is a 54.4% probability that the lightning occurred within that radius.

FIG. 12. Google Maps visualization of the 99% confidence uncertainty ellipse for a lightning strike near Complex 39A on 03 August 2009. Figure 12 shows a probability of 10.4% of the lightning strike occurring within the 0.45 nmi radius.

FIG. 13. Google Maps visualization of the 99% confidence uncertainty ellipse for a lightning strike near Complex 39A on 03 August 2009. Figure 13 shows a probability of 6.4% of the lightning strike occurring within the 0.45 nmi radius.

FIG. 14. Google Maps visualization of the 99% confidence uncertainty ellipse for nearby lightning strike to Complex 39A on 03 August 2009. Figure 14 shows a probability of 0.7% of the lightning strike occurring within the 0.45 nmi radius.

FIG. 15. Google Maps visualization of the 99% confidence uncertainty ellipse for a lightning strike near Complex 39A on 03 August 2009. Figure 15 shows a probability of 7.3% of the lightning strike occurring within the 0.45 nmi radius.

FIG. 16. Illustrates a probability of 92.1% of a lightning strike of amplitude -38.9 kA detected by CGLSS occurring 0.32 nmi from the center of Launch Complex 39A on 8/16/2009.

FIG. 17. Illustrates a probability of 72.1% of a lightning strike of amplitude -43.0 kA detected by NLDN occurring 0.26 nmi from the center of Launch Complex 39A on 8/16/2009.

FIG. 18. Illustrates a probability of 77.7% of a lightning strike of amplitude -71.4 kA detected by NLDN occurring 0.28 nautical miles from the center of Launch Complex 39A on 10/14/2009.

FIG. 19. Illustrates a probability of 97.2% of a lightning strike of amplitude -39.5 kA detected by CGLSS occurring 0.12 nmi from the center of Launch Complex 39A on 7/21/2008.

FIG. 20. Illustrates a probability of 99.999975% of a lightning strike of amplitude -18.9 kA detected by CGLSS occurring 0.03 nmi from the center of Launch Complex 39B on 6/27/2009.

FIG. 21. Illustrates a probability of 99.999925% of a lightning strike of amplitude -21.7 kA detected by CGLSS occurring 0.04 nmi from the center of Launch Complex 39B on 6/27/2009.

TABLE 1. Calculated probability vs. CRC Handbook probability for various inputs.

Semi-major Axis (nmi)	Semi-minor Axis (nmi)	Heading of semi-major axis from true North	Point Of Interest latitude	Point Of Interest long-itude	Strike Latitude	Strike Long-itude	Radius around Point Of Interest (nmi)	Calcu-lated prob-ability	CRC Hand-book prob-ability [4]
3	3	15	28.6082	-80.6041	28.6995	-80.6041	3	0.095	0.095
3	3	15	28.6082	-80.6041	28.631	-80.6041	3	0.453	0.452
3	3	15	28.6082	-80.6041	28.608	-80.6041	3	0.500	0.499
1	1	15	28.6082	-80.6041	28.608	-80.6041	1	0.500	0.499
1	1	15	28.6082	-80.6041	28.631	-80.6041	1	0.200	0.200
1	1	15	28.6082	-80.6041	28.6995	-80.6041	1	0.000	0.000
1	1	15	28.6082	-80.6041	28.608	-80.6041	2	0.937	0.938

TABLE 2.. Input values used for scenarios shown in Figures 2 through 8.

Figure	Semi-major axis of 50% Confidence Ellipse (nmi)	Semi-minor axis of 50% Confidence Ellipse (nmi)	Confidence	Heading (from true North) of semi-major axis	Point Of Interest latitude (°N)	Point Of Interest longitude (°W)	Strike latitude (°N)	Strike longitude (°W)	Radius around Point Of Interest (nmi)
2	3.1	1.2	0.50	75	28.60827	80.6041	28.59	80.59	Varied
3	0.3	0.2	0.50	44.3	28.60827	80.6041	Varied	80.6041	0.45
4	0.3	0.2	0.50	44.3	28.60827	80.6041	28.6082	Varied	0.45
5	0.3	0.2	0.50	Varied	28.60827	80.6041	28.6162	80.6041	0.45
6	0.3	0.2	0.50	180	28.60827	80.6041	28.6162	80.6041	0.45
7	0.3	0.2	0.50	90	28.60827	80.6041	28.6162	80.6041	0.45
8	Varied	0.1	0.50	90	28.60827	80.6041	28.6062	80.6041	0.45

TABLE 3. Input values used for scenarios shown in Figures 10 through 15.

Figure	Semi-major axis of 50% Confidence Ellipse (nmi)	Semi-minor axis of 50% Confidence Ellipse (nmi)	Confidence	Heading (from true North) of semi-major axis	Point Of Interest latitude (°N)	Point Of Interest longitude (°W)	Strike latitude (°N)	Strike longitude (°W)	Radius around Point Of Interest (nmi)
10	0.15	0.05	0.99	301.5	28.60827	80.6041	28.6107	80.6124	0.45
11	0.2	0.1	0.99	300.7	28.60827	80.6041	28.6114	80.6113	0.45
12	0.15	0.05	0.99	301.3	28.60827	80.6041	28.6122	80.6147	0.45
13	0.15	0.1	0.99	293	28.60827	80.6041	28.6178	80.6069	0.45
14	0.6	0.2	0.99	88.8	28.60827	80.6041	28.6041	80.6317	0.45
15	0.3	0.2	0.99	293	28.60827	80.6041	28.6178	80.6069	0.45

TABLE 4. Input values used for scenarios shown in Figures 16 through 21.

Figure	Semi-major axis of 50% Confidence Ellipse (nmi)	Semi-minor axis of 50% Confidence Ellipse (nmi)	Confidence	Heading (from true North) of semi-major axis	Point Of Interest latitude (°N)	Point Of Interest longitude (°W)	Strike latitude (°N)	Strike longitude (°W)	Radius around Point Of Interest (nmi)
16	0.15	0.05	0.99	300.8	28.60827	80.6041	28.6105	80.5987	0.45
17	0.3	0.2	0.99	82	28.60827	80.6041	28.6069	80.6087	0.45
18	0.2	0.2	0.99	95	28.60827	80.6041	28.6057	80.6085	0.45
19	0.2	0.1	0.99	49	28.60827	80.6041	28.6064	80.6050	0.45
20	0.1	0.05	0.99	70	28.62716	80.6208	28.6277	80.6207	0.45
21	0.1	0.05	0.99	72	28.62716	80.6208	28.6275	80.6202	0.45

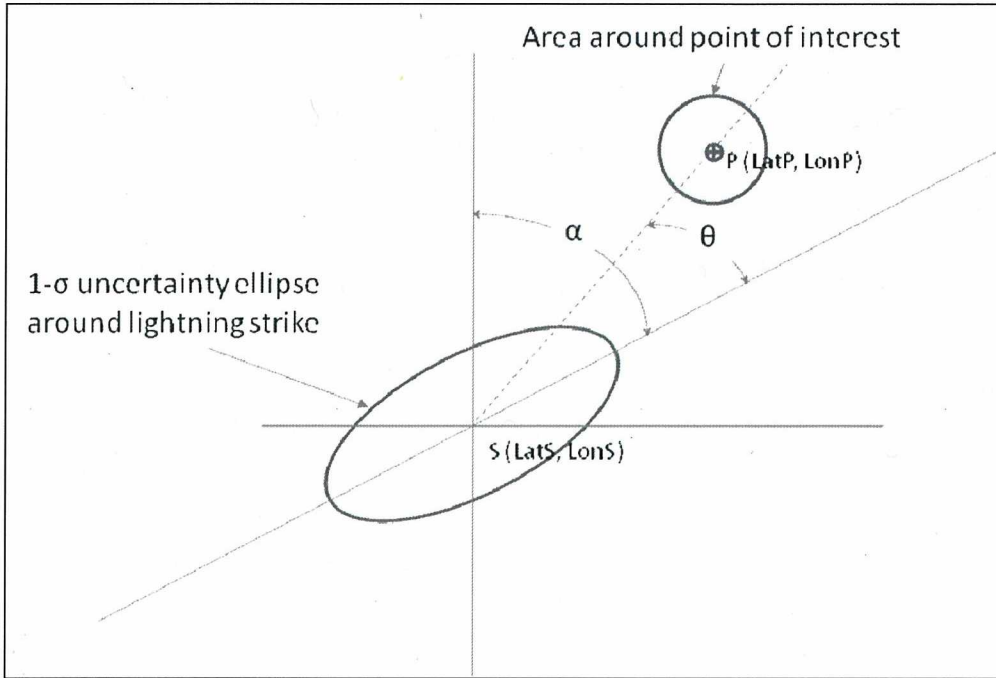


FIG. 1. Schematic diagram of the angles used in probability calculation for a sample lightning location error ellipse. α is the heading of the semi-major axis of the lightning location uncertainty ellipse from true north. θ is the angle between the semi-major axis of the lightning location uncertainty ellipse and line connecting the center of the lightning uncertainty ellipse and the center of the area of interest.

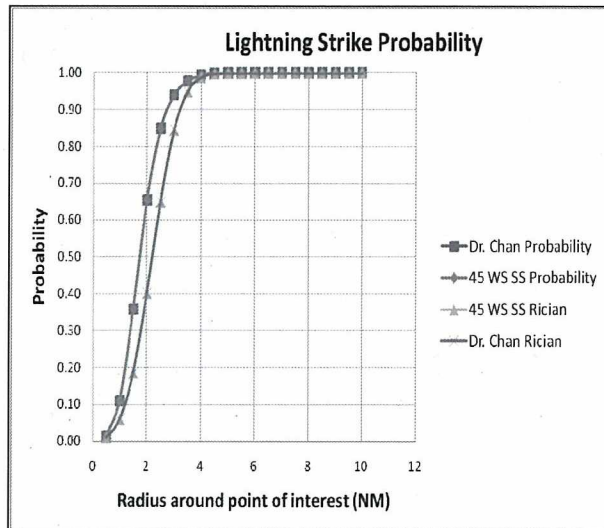


FIG. 2. Change in probability as a result of changing the point of interest radius while holding all other parameters constant.

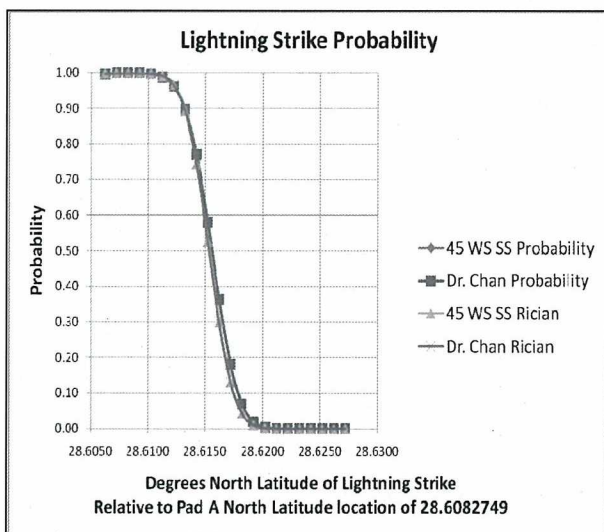


FIG. 3. Change in probability as a result of changing the latitude of the strike from the point of interest while holding all other parameters constant.

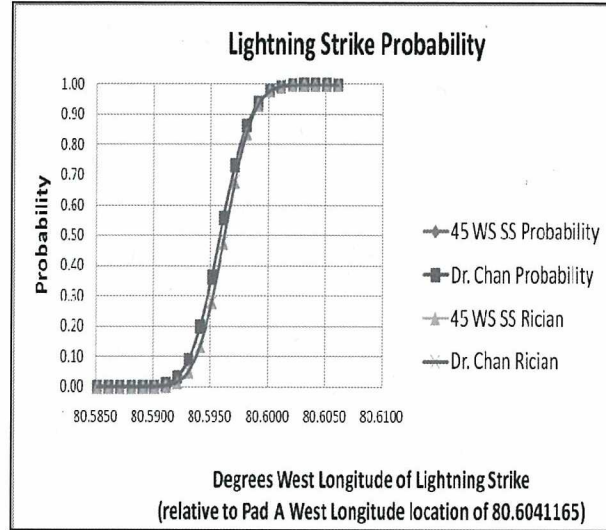


FIG. 4. Change in probability as a result of changing the longitude of the strike from the point of interest while holding all other parameters constant.

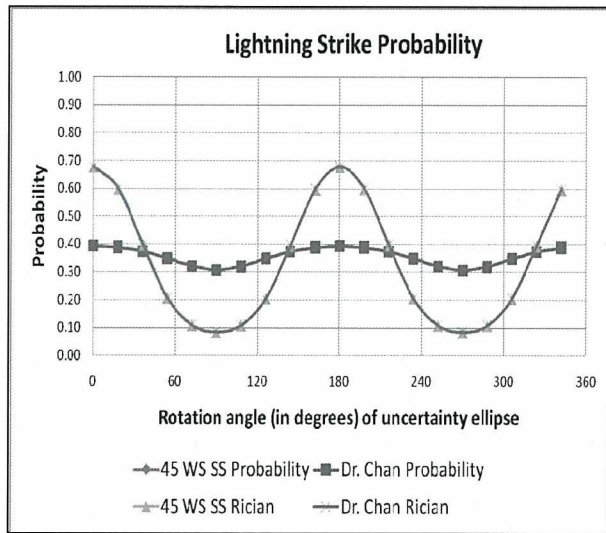


FIG. 5. Change in probability as a result of changing the semi-major axis heading of the lightning uncertainty ellipse while holding all other parameters constant.



FIG. 6. Google Maps visualization of a lightning uncertainty ellipse overlaid on the radius around the point of interest with a semi-major axis heading of 180° as graphed in Figure 5.



FIG. 7. Google Maps visualization of a lightning uncertainty ellipse overlaid on the radius around the point of interest with a semi-major axis heading of 90° as graphed in Figure 5.

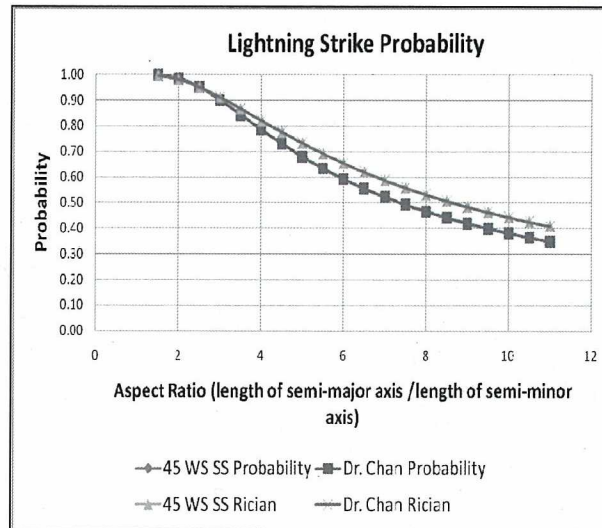


FIG. 8. Change in probability as a result of varying the aspect ratio (length of semi-major axis/length of semi-minor axis) of the lightning uncertainty ellipse from 1.5 to 11 with the strike point close to the point of interest while holding all other parameters constant.

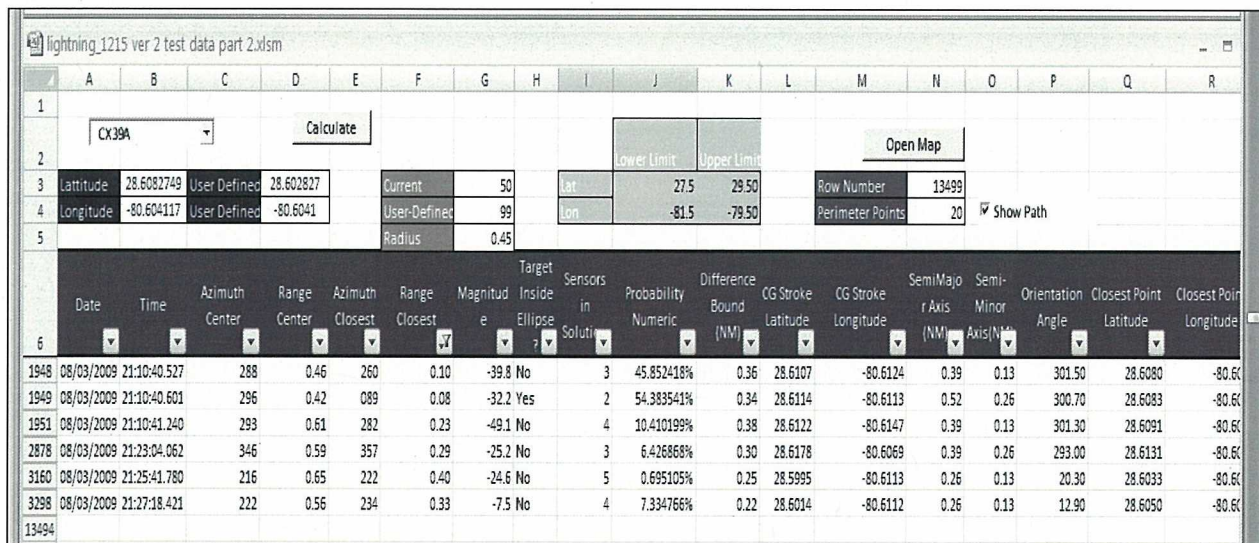


FIG. 9. Sample of lightning strikes where the closest point on the lightning position uncertainty ellipse was within 0.45 nmi of Launch Complex 39A on 3 August 2009.

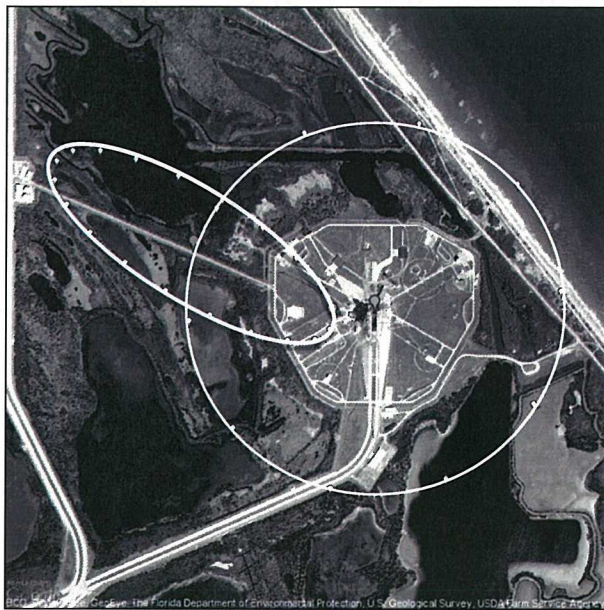


FIG. 10. Google Maps visualization of the 99% confidence uncertainty ellipse for the closest lightning strikes to Complex 39A on 03 August 2009. There is a 45.9% probability that the lightning strike occurred within the 0.45 nmi radius.



FIG. 11. Google Maps visualization of the 99% confidence uncertainty ellipse for one of the closest lightning strikes to Complex 39A on 03 August 2009. The center of the ellipse was within the 0.45 nmi radius. There is a 54.4% probability that the lightning occurred within that radius.

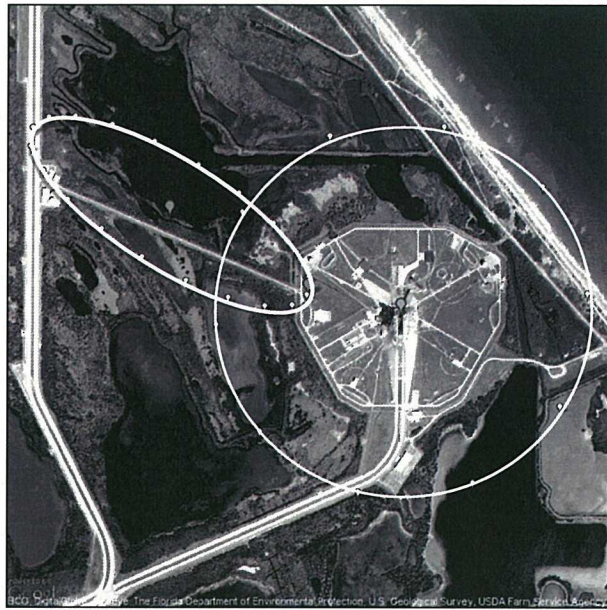


FIG. 12. Google Maps visualization of the 99% confidence uncertainty ellipse for a lightning strike near Complex 39A on 03 August 2009. Figure 12 shows a probability of 10.4% of the lightning strike occurring within the 0.45 nmi radius.

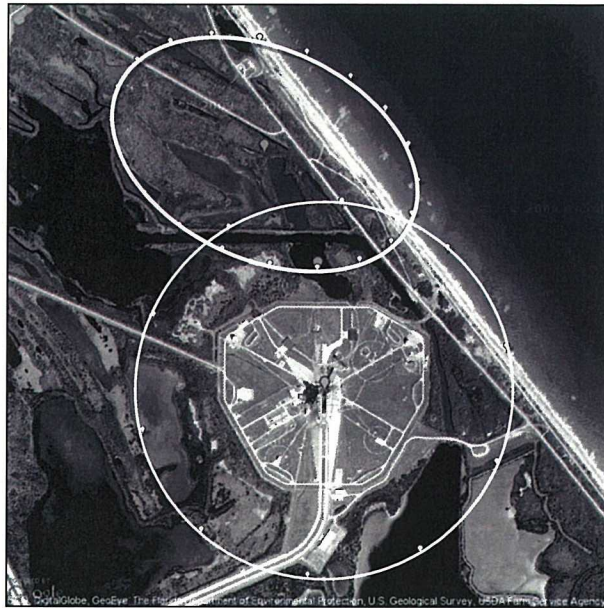


FIG. 13. Google Maps visualization of the 99% confidence uncertainty ellipse for a lightning strike near Complex 39A on 03 August 2009. Figure 13 shows a probability of 6.4% of the lightning strike occurring within the 0.45 nmi radius.

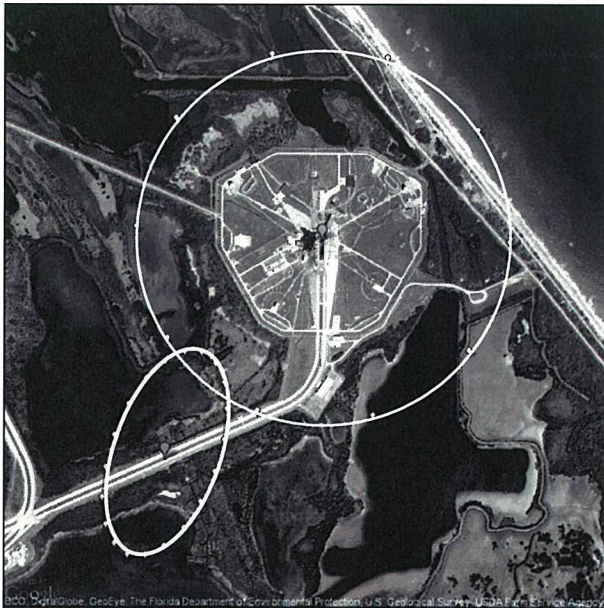


FIG. 14. Google Maps visualization of the 99% confidence uncertainty ellipse for nearby lightning strike to Complex 39A on 03 August 2009. Figure 14 shows a probability of 0.7% of the lightning strike occurring within the 0.45 nmi radius.



FIG. 15. Google Maps visualization of the 99% confidence uncertainty ellipse for a lightning strike near Complex 39A on 03 August 2009. Figure 15 shows a probability of 7.3% of the lightning strike occurring within the 0.45 nmi radius.

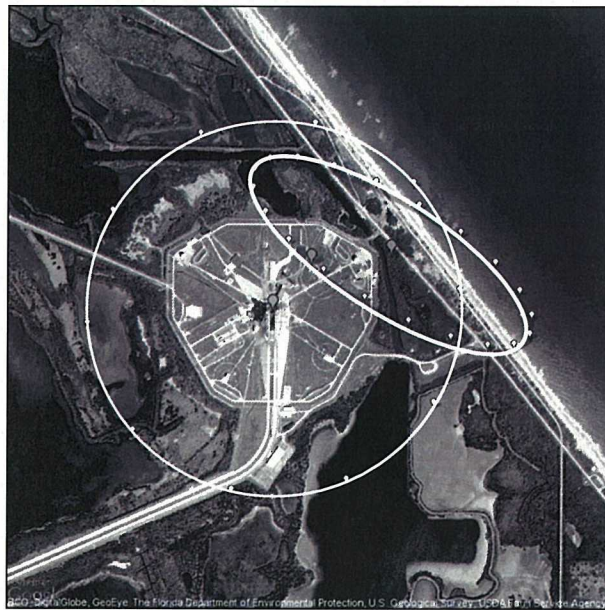


FIG. 16. Illustrates a probability of 92.1% of a lightning strike of amplitude -38.9 kA detected by CGLSS occurring 0.32 nmi from the center of Launch Complex 39A on 8/16/2009.



FIG. 17. Illustrates a probability of 72.1% of a lightning strike of amplitude -43.0 kA detected by NLDN occurring 0.26 nmi from the center of Launch Complex 39A on 8/16/2009.



FIG. 18. Illustrates a probability of 77.7% of a lightning strike of amplitude -71.4 kA detected by NLDN occurring 0.28 nautical miles from the center of Launch Complex 39A on 10/14/2009.



FIG. 19. Illustrates a probability of 97.2% of a lightning strike of amplitude -39.5 kA detected by CGLSS occurring 0.12 nmi from the center of Launch Complex 39A on 7/21/2008.

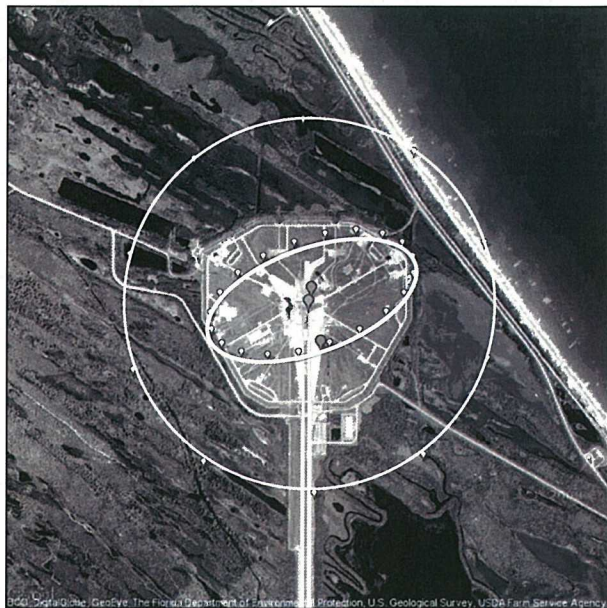


FIG. 20. Illustrates a probability of 99.999975% of a lightning strike of amplitude -18.9 kA detected by CGLSS occurring 0.03 nmi from the center of Launch Complex 39B on 6/27/2009.

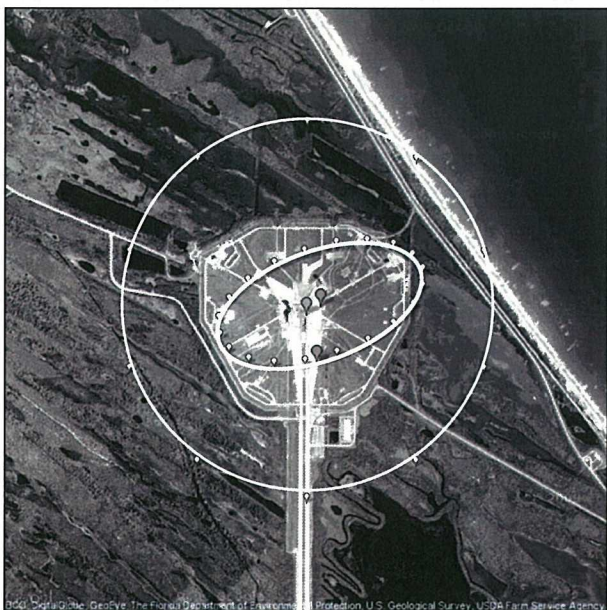


FIG. 21. Illustrates a probability of 99.999925% of a lightning strike of amplitude -21.7 kA detected by CGLSS occurring 0.04 nmi from the center of Launch Complex 39B on 6/27/2009.